RELATIONSHIP BETWEEN CHEMICAL AND STRUCTURAL FEATURES OF TOPAZ TO UNRAVEL THE FORMATION CONDITIONS: A MULTIDISCIPLINARY APPROACH

NICOLA PRECISVALLE
Dipartimento di Fisica e Scienze della Terra, Università di Ferrara, Via Saragat 1, 44124 Ferrara

INTRODUCTION AND AIM OF THE WORK

Topaz, $Al_2SiO_4(OH,F)_2$, is one the main fluorine bearing silicates that occurs as accessory minerals in fluorine rich silicates rocks associated with magmatic or hydrothermal events (Alberico *et al*., 2003; Zhang *et al*., 2011). In some cases, it can also be a principal component in some peculiar rocks called "topazite" (or topaz rhyolites) (Kortemeier & Burt, 1988; Burt *et al*., 1982; Soufi, 2021) and topaz ongonite (Burt *et al*., 1982; Soufi, 2021). Because of this characteristic, topaz deposits are spread worldwide and can form in very different environment. The structure consists of $[SiO_4]^{4-}$ groups linking octahedral chains of $Al[O_4(F, OH)_2]$ in a zig-zag arrangement parallel to the c-axis. Four out of the six anions surrounding the Al^{3+} ion belong to $[SiO_4]^{4-}$ tetrahedra; and two form F - or OH - groups (Fig. 2 a, b). Natural topaz crystallizes in the orthorhombic *Pbnm* space group; pronounced sectoral textures with growth planes {hkl} optically triclinic, {0kl}, {k0l}, and {hk0} optically monoclinic, and {100}, {010}, and {001} optically orthorhombic are also well documented. (Precisvalle *et al*., 2021).

By the way, this mineral is not only an important petrologic indicator, but also a well renowned gemstone that since ancient times is searched and desired by people for its beauty. From the literature, the main method to distinguish topazes of different origins is to determine the OH/F ratio (Ribbe & Gibbs, 1971; Ribbe & Rosenberg, 1971; Wunder *et al*., 1999). To do this, methods based on the study of the structure of topaz have so far been used, through correlations between the measurement of its cell parameters (*b* parameter and unit cell volume) and the estimation of the weight percentage of F, then obtaining the OH content by difference (Ribbe & Rosenberg, 1971; Alberico *et al*., 2003). However, this method, although effective when comparing a small number of samples, proves to be deficient when the number of topazes of certain origin increases and compared with each other. In addition, another limitation of this methodology is that it does not consider the various types of deposits, which, as mentioned above, differ greatly in the chemistry and temperature of the magmas or hydrothermal fluids. In this work two topaz "families" from different origin, natural blue topaz from Padre Paraíso municipality (Brazil) and colourless topaz from Baoshan county (China), has been fully characterized in terms of geochemical and crystallographic features in order to explore the relationships between structure (*i.e*., OH/F substitution) and environmental conditions. The aim of this work is to establish a correlation between OH/F ratio and formation chemical environment in relation to the efficiency of the mineral/fluid partitioning process in topazes and in the end, define a model to explain the accommodation of elements in the crystal structure as function of the geological environment, thus possibly determine the gem identity and provenance.

MATERIALS

Padre Paraíso blue topaz (PadPar)

The blue topaz crystals studied in this work have been collected in the Padre Paraíso municipality, located in the North-East area of Minas Gerais State in Brazil. The whole area belongs to the Late Neoproterozoic-Cambrian Araçuaí orogen, a great orogenic body that show up in the eastern part of Brazil (Pedrosa-Soares *et al.*, 2011). The pegmatitic district belonging to this orogeny form the Eastern Brazilian Pegmatite Province (EBPP) (Pedrosa-Soares *et al.*, 2011; Precisvalle *et al*., 2021). The granite that form the EBPP has been grouped in 5 different supersuites, characterized by different age, geochemical data and structural features called G1 to G5 (De

Campos *et al*., 2004; Pedrosa-Soares *et al*., 2011). The blue topaz samples come from the G5 supersuite. The Padre Paraíso topaz in this study are all centimetric in size, from 1 to 2 cm, with irregular shape and no recognizable form; they present a clear to intense light blue colouration, with no fades or colour flaws in all the samples collected. All crystals have good transparency with medium-high clarity. They are very poorly to poorly included, with solid and biphasic inclusions. The solid inclusions are sporadic and are mostly represented by small quartz, micas and very rare sulphides and oxides.

Baoshan colourless topaz (Bao)

The colourless topaz studied in this work comes from the Baoshan ores area in the Yunnan province of China. It is part of the Sanjiang region that comprehend the SE Tibet Plateau and the NW Yunnan, formed from the amalgamation of the Gondwana derived continental blocks and arc terranes as a result of oceanic subduction that occurred before the late Paleozoic tectonic events that lead to the continental collision. (Deng *et al*., 2014) The topaz deposits in the Yunnan province are related to the Thetys Sn metallogenic domain, in particular the Tengchong-Baoshan block with its hydrothermal vein type mineralization. The magmatism is dominated by crustal melting (S-type granitoids) with an age that ranges from Early Cretaceous to Late Cretaceous/Early Cenozoic (Wang *et al*., 2013). In Tengchong and Baoshan there are eight principal metallic deposits, bearing Sn, Nb, Ta and Li all related to low metamorphization due to hydrothermal fluids. The Baoshan topaz run from small chips to bigger euhedral samples. All crystals have a good transparency and high clarity; the solid inclusions are predominant, the most recognizable are tantalite, quartz, tourmaline, oxides and sulphides.

METHODS

Synchrotron X-ray powder diffraction

The powdered topazes were poured into a thin-walled boron capillary (diameter 0.5 mm) and then collected in transmission geometry (monochromatic wavelength of 0.827 Å, 15 keV) and 1×0.3 mm^2 spot size at the MCX beamline of Elettra - Synchrotron Trieste, (Italy). They were then mounted on a standard goniometric head and spun during data collection. Powder diffraction patterns were collected in 10°-65° 2θ range with a step size of 0.008° and an exposure time of 1 s. Each sample was subjected to the same heat treatment; samples were heated from room temperature to 1273 K with a heating rate of 5 K/min using a hot gas blower directing a hot air flux onto the spinning quartz-capillary. Diffraction data were collected every 50 K. The temperature was continuously measured by a thermocouple and calibrated using the quartz thermal expansion and phase transition.

Neutron powder diffraction

Neutron Powder Diffraction (NPD) experiments were then carried out on the high-flux two-axis neutron powder diffractometer D20 at the Institute Laue Langevin (ILL, Grenoble, France) using the same topaz sample. Useful data were collected between 6 and 142 degrees, of which 22 to 142 degrees were treated as follow. The samples were heated *in situ* under flowing gas (5% H_2/He), from room temperature to 1273 K (heating rate 2 K/min). Data sets were collected for 2 minutes, thus covering 4 K. A wavelength of 1.54 Å was chosen, from a germanium-(115) monochromator at 90° take-off angle. The sample was poured into a 4 mm diameter vanadium cylinder, placed in the centre of the furnace's vacuum vessel, and heated by a 30 mm diameter vanadium resistor (Martucci & Hansen, 2019). A type-K thermocouple was in the centre of the furnace to calibrate the temperature. The same configuration was maintained during all data collection. A set of diffraction patterns were obtained with this procedure as a function of temperature.

Scanning electron microscope (SEM)

For this study, both populations were analysed with a CAMSCAN MX 2500 Scan Electron Microscope (SEM) with an EDAX system for Energy Dispersive Analyses. The SEM was equipped with a high brightness LaB6 cathode, operating in a high vacuum. The samples were coated with carbon. For quantitative purposes, a set of natural minerals was used as standards for their specific elements: augite (Si and Ca), fluorite (F), gahnite (Al)

and olivine (Mg, Fe). Relative analytical errors (1σ) of major elements were below 1.00% for Si and for Al; and 3.00-6.00% for F. Images were collected both in SEI (Secondary Electron Imaging) and BEI (Backscattered Electron Imaging). The parameters used for the analyses were EHT 20 kV, EMI 71 μA, FIL 1.80 A with a working distance of 25 mm. Imaging and measurements were performed at the Microscopy Laboratory of the University of Padova.

Laser Ablation - Inductively Coupled Plasma Mass Spectrometry (LA-ICP-MS)

The chemical characterization for trace elements for both populations has been obtained by mean of LA-ICP-MS. In order to carry out *in situ* chemical analyses of the samples a section had to be made. The obtained thin cross-sections generally have a thickness of 0.4 cm with an average diameter of 1 cm. Raw samples has been polished with a diamond disk and then with diamond suspension. The sections have been prepared at the Sample Preparation Lab at University of Ferrara. Trace elements were analysed by (LA-ICP-MS) using an Agilent 8900 Triple Quadrupole ICP-MS, coupled to a GeoLas200 Microlas Eximer laser with a wavelength of 193 nm using an ArF gas. The measurements have been carried out at the IGG (*Istituto di Geoscienze e Georisorse*) - CNR (*Centro Nazionale delle Ricerche*), Pavia (Italy). The spot size was 50 μm. Fluorine combined with argon was a carrier gas and ablation have been carried out with a pulse rate of 10 Hz and an energy density of 8 J/cm^2. The LA-ICP-MS data collection have provided 60 s of background acquisition followed by 70 s of ablation. The software GLITTER 4.0 has been used for data reduction with NIST 610 and NIST 612 as primary external standard, BCR – 2 g as second external standard and ^{29}Si as internal standard.

TwinMic: Soft X-ray Transmission and Emission Microscope

Low energy X-ray fluorescence (LEXRF) analyses were performed at TwinMic beamline of Elettra Synchrotron Trieste. The incident X-ray beam energy was 2 keV to ensure the best excitation and detection of the Kα lines of Si, Al, Ga, Ge, As and F atoms. The samples were raster-scanned with a step size of 0.8 μm across a microprobe of 0.8 μm diameter delivered by a 600 μm diameter Au zone plate optics with 50nm outermost zone. XRF maps were acquired on areas of around 76 μm × 76 μm or 72 μm × 72 μm, with 5 s/pixel acquisition time and were process with PYMCA software package. These energies of acquisition needs samples with large surface, but 5 microns maximum thickness. This condition applied on solid crystalline state is quite challenging. The sample preparation procedure has been specifically developed for this study and, as far as I know, never applied before on this material. The samples have been prepared at Center for Electron Microscopy at *Istituto Officina dei Materiali* - CNR Trieste. The samples have been prepared with the Precision Ion Polishing System (PIPS). It is based on a technique that produces discs with a diameter of 3 mm that can be thinned mechanically down to about 50 microns. The disc is then thinned in the central area (using a dimpler) to create a crater geometry with a thickness that varies from the outside to the inside (from 50 microns on the outside to 25 microns in the centre). This disc is then placed in an ion bombardment system to thin the central zone until a hole is created in the centre. The thinnest zone will be the one around the hole, which has a thickness of up to 50 nm at the very edge of the hole. The crater geometry is preserved: the thickness increases from the inside to the outside. The so-obtained samples have been mounted on a Cu TEM grid for focusing.

RESULTS

The successful strategy to combine EDS microanalyses with synchrotron X-ray and neutron powder diffraction *in situ* measurements (from RT to 1273 K) allowed to accurately determine the mineral structure of topaz, and to reconstruct backwards both the environment and the possible conditions of formation. The results, then, have been subsequently supported by the trace element analysis and the micro-XRF mapping helped to better understand the setting-up for trace elements on topazes' surface.

The fluorine content obtained from the EDS analyses reveals an average F content of ~1.05 a.f.u for Padre Paraíso topaz and ~1.53 a.f.u. for the Baoshan topaz.

These values are in pretty good agreement with those estimated from the refined occupancies of neutron diffraction data of ~1.03 a.f.u (Padre Paraíso) and ~1.59 a.f.u (Baoshan) with OH/(OH+F) = 0.484 (Padre Paraíso) and 0.24 (Baoshan) (Table 1).

Table 1. Cell parameters and calculated a.f.u. from refined F site for Padre Paraiso and Baoshan topaz at room temperature.

Cell parameters (RT)	**Synchrotron PadPar**	**Synchrotron Bao**	**Neutron PadPar**	**Neutron Bao**
a	4.6524(1) Å	4.6493(1) Å	4.6445(1) Å	4.6406(1) Å
b	8.8048(1) Å	8.7964(1) Å	8.7877(1) Å	8.7767(1) Å
c	8.3894(1) Å	8.3901(1) Å	8.3742(1) Å	8.3743(1) Å
Vol	343.65(1) Å^3	343.13(1) Å^3	341.79(1) Å^3	341.08(1) Å^3
a.f.u F			1.032	1.599

The study of trace elements by means of micro-XRF mapping showed good results about distribution of major and trace elements on topaz surface. Indeed, here for the first time it has been possible to have a direct observation of elemental substitution in tetrahedral and octahedral site and elemental adsorption. In particular, in the correlograms and the colour maps: demonstrated the random distribution of O and F in octahedra, Al-Ga and Si-Ge substitution has been observed; they showed a random distribution along the topazes' surface, Arsenic, for the first time, has been shown to be included in topaz either as a substitute for Si (as in the case of Padre Paraíso topaz) or absorbed in the cavities between octahedrons (as in Baoshan topaz). The *in situ* analyses from both neutron and synchrotron data showed an expansive trend for the topaz structure evolution through heating (Fig. 1 a, b, c, d).

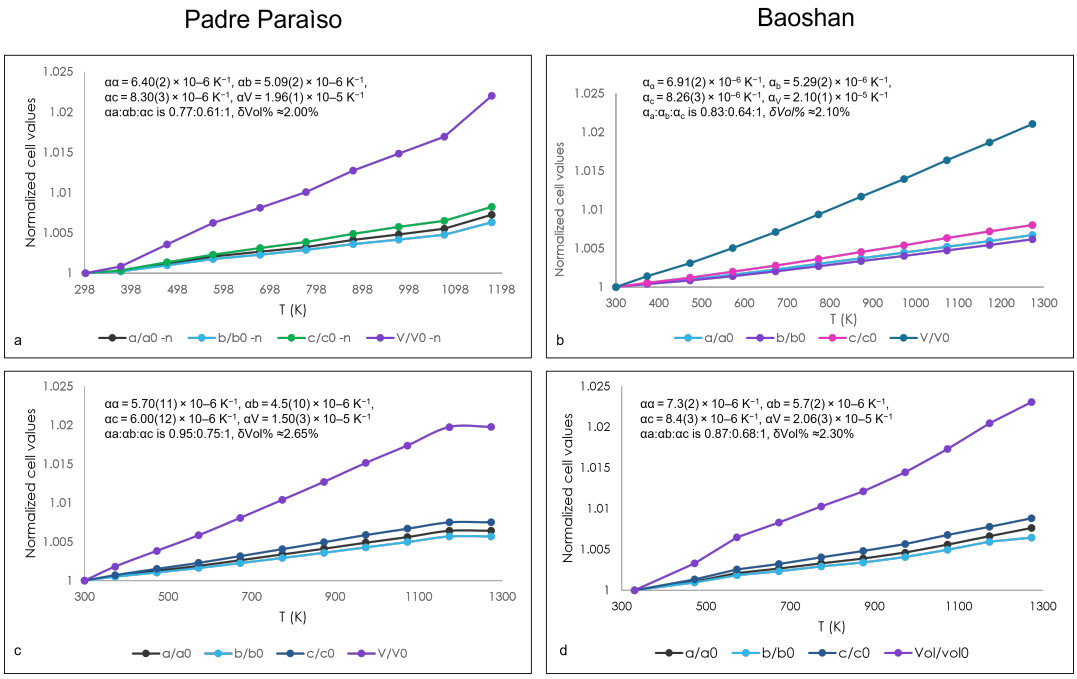

Fig. 1 - Evolution of unit cell parameters for Padre Paraiso and Baoshan topaz normalized with respect to room temperature values (a/a0, b/b0, c/c0, V/V0) from *in situ* synchrotron (a, c) and neutron diffraction (b, d) data. Standard deviation errors are within the symbol size. The thermal expansion coefficients (calculated from Fei, 1995) has investigated for both samples from 298 to 1273 K using the EosFit7-GUI software (Gonzalez-Platas *et al.*, 2016) and are reported on the graphs.

From *in situ* neutron diffraction, the appearance of mullite phase is observed at different temperature in the two topaz populations (1181 K and 1225 K for Padre Paraíso and Baoshan, respectively). In this work, for the first time the progressive transformation of topaz into mullite was recorded by diffraction analyses unlike previously, where this transformation was only observed at the end of a calcination cycle (Day *et al.*, 1995; Miao, 1999; Monteiro & Sabioni, 2014).

The temperatures obtained thus were interpreted as the potential temperatures for the crystallisation of a topaz, depending on the amount of fluorine in the structure, and thus on the fluorine availability in the environment in which the topaz crystallises (Fig. 2 a, b).

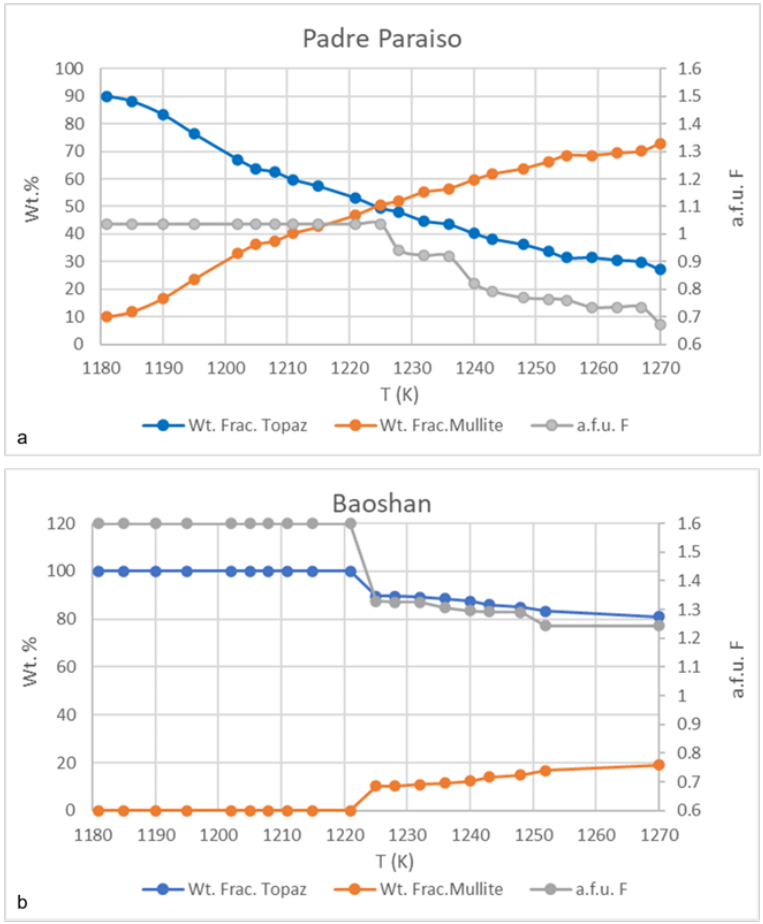

Fig. 2 - Fluorine behaviour in topaz-mullite transition zone for Padre Paraìso (a) and Baoshan (b) topaz from neutron diffraction refinements. F atoms in topaz (atomic formula unit, a.f.u.: grey pattern); weight fractions (wt. fract.) patterns of topaz and mullite in blue and orange, respectively.

So, from these temperatures and F contents obtained from the neutron diffraction it has been possible to reconstruct the nature of topaz forming fluid system. In order to do this, it has been modified the Barton (1982) equation for biotite and adapted to topaz. The fluorine content, expressed as the ratio $\log(f\mathrm{H_2O}/f\mathrm{HF})_{\mathrm{fluid}}$, of possible fluids (or $\mathrm{H_2O}$-F saturated silicic melt) coexisting with the topaz, was modelled based on the partitioning of F-(Cl)-OH behaviour between fluorine bearing minerals and late- post magmatic pegmatitic fluids/greisenization reaction. In such a view, it is possible to infer that Padre Paraíso topaz nucleated at ~1148-1181 K from a water rich /fluorine poor fluid ($(f\mathrm{H_2O}/f\mathrm{HF})_{\mathrm{fluid}}$ ~ 4.5 log units). This value is coherent with a OH/F ratio as observed in typical pegmatitic-hydrothermal type fluids (Barton,1982; Dolejš & Baker, 2004); instead Baoshan topaz started to form at higher temperature ~1203-1225 K from a water poor /fluorine rich fluid ($(f\mathrm{H_2O}/f\mathrm{HF})_{\mathrm{fluid}}$ ~ 1.2 log units).

This lower value (and relatively high temperature of topaz formation) suggests that Baoshan forming fluids is more influenced by fluorine activity as observed for late magmatic fluid that acts as metasomatic agents for the greisenitazion reactions. (Barton, 1982; Dolejš & Baker, 2004). Coherently with the F/OH topaz ratios, the topaz-forming fluids of Padre Paraìso is richer in water compared to Baoshan. The remarkable high of Li, Be and B and low Ge contents confirms the pegmatite origin of the Padre Paraìso blue topaz, in agreement with the pegmatite type composition as reported for Padre Paraìso topaz deposits (Černý, 1991; Zagorsky *et al*., 1999; Černý & Ercit, 2005; Martin & De Vito, 2005; Müller-Lorch *et al*., 2007; Pedrosa-Soares *et al*., 2011). Another good hint of pegmatitic origin is the Fe content, that is a strong geochemical signature of Padre Paraíso gemstones mineralization and like in Padre Paraíso aquamarine, could be related to the strong light-blue coloration (Achtschin, 1999; Gandini *et al*., 2001; Ferreira *et al*., 2005; Kahwage & Mendes, 2003; Pedrosa-Soares *et al*., 2011).

The Baoshan topaz has higher contents of Ge with respect to Padpar topaz. Germanium is main vicariant element for Si (and to lesser extent Al), that is a typical enrichment for minerals from greisen-type deposits from alteration of S-type granites (Breiter *et al*., 2014; Launay *et al*., 2021). This result is perfectly in line with that reported by Guo *et al.* (2011), who in their study on the tin ore deposits of the Tengchong-Baoshan block analyse the granitoids in the area of origin of our samples and describe them as originating from S-type granites. Other indicators of the greisen origin of Baoshan topaz are the presence of Fe and Ti, Ga and the related depletion of Zn, W and Sn that crystallise into other phases such as cassiterite and other oxides (Breiter *el al*., 2014; Guo *et al*., 2011; Launay, 2021). The greisen deposit origin for the Baoshan topaz and allows us to reduce the number of possible source deposits presents in the Tengchong-Baoshan Sn-polymetallic metallogenic belt from eight (counting only the main deposits) to four, the greisen type deposits, namely: Baihuanao, Xiaolonghe, Dasongpo and Lailishan (Li *et al*., 2009; Wang *et al*., 2013).

REFERENCES

Achtschin, A.B. (1999): Caracterização geológica, mineralógica e geoquímica dos pegmatitos do Distrito de Padre Paraíso, Minas Gerais, e suas variedades de berilo. MSc thesis, Instituto de Geociências, Universidade Federal de Minas Gerais, Brazil.

Alberico, A., Ferrando, S., Ivaldi, G., Ferraris, G. (2003): X-ray single-crystal structure refinement of an OH-rich topaz from Sulu UHP terrane (Eastern China) - Structural foundation of the correlation between cell parameters and fluorine content. *Eur. J. Mineral*., **15**, 875-881.

Barton, M.D. (1982): The thermodynamic properties of topaz solid solutions and some petrologic applications. *Am. Mineral*., **67**, 956-974.

Breiter, K., Ackerman, L., Ďurišová, J., Svojtka, M., Novák, M. (2014): Trace element composition of quartz from different types of pegmatites: A case study from the Moldanubian Zone of the Bohemian Massif (Czech Republic). *Mineral. Mag*., **78**, 703-722.

Burt, D.M., Sheridan, M.F., Bikun, J.V., Christiansen, E.H. (1982): Topaz rhyolites; distribution, origin, and significance for exploration. *Econ. Geol.*, **77**, 1818-1836.

Černý, P. (1991): Rare-element granitic pegmatites. Part I: Anatomy and internal evolution of pegmatite deposits. *Geosci. Canad.*, **18**, 49-67.

Černý, P. & Ercit, T.S. (2005): The classification of granitic pegmatites revisited. *Canad. Mineral.*, **43,** 2005-2026.

Day, R.A., Vance, E.R., Cassidy, D.J., Hartman, J.S. (1995): The topaz to mullite transformation on heating. *J. Mater. Res*., **10**, 2963-2969.

De Campos, C.D., Mendes, J.C., Ludka, I.P., Medeiros, S.R., Moura, J.C., Wallfass, C. (2004): A review of the Brasiliano magmatism in southern Espírito Santo, Brazil, with emphasis on postcollisional magmatism *J. Virtual Explor*., **17**, 35.

Deng, J., Wang, Q., Li, G., Li, C., Wang, C. (2014): Tethys tectonic evolution and its bearing on the distribution of important mineral deposits in the Sanjiang region, SW China. *Gondwana Res.*, **26**, 419-437.

Dolejš, D. & Baker, D.R. (2004): Thermodynamic analysis of the system Na_2O-K_2O-CaO-Al_2O_3-SiO_2-H_2O-F_2O_{-1}: Stability of fluorine-bearing minerals in felsic igneous suites. *Contrib. Mineral. Petrol.*, **146**, 762-778.

Fei, Y. (1995): Thermal expansion. *In*: "Mineral Physics and Crystallography: A Handbook of Physical Constants - Vol. 2", T.J. Ahrens, ed. AGU, Washington D.C., 29-44.

Ferreira, M.S.F., Fonseca, M.A., Pires, F.R.M. (2005): Pegmatites mineralized in aqua marine and topaz of Ponto do Marambaia, Minas Gerais: tipology and relationships with the Caladão granite. *Rev. Bras. Geociênc*., **35**, 463-473.

Gandini, A.L, Achtschin, A.B., Marciano, V.R., Bello, R.F., Pedrosa-Soares, A.C. (2001): Berilo. *In*: "Gemas De Minas Gerais, Belo Horizonte", C. Castañeda, J.E. Addad, A. Liccardo, eds. Sociedade Brasileira De Geologia Núcleo Minas Gerais, 100-127.

Gonzalez-Platas, J., Alvaro, M., Nestola, F., Angel, R. (2016): EosFit7-GUI: a new graphical user interface for equation of state calculations, analyses and teaching. *J. Appl. Cryst*., **49**, 1377-1382.

Guo, C., Mao, J., Bierlein, F., Chen, Z., Chen, Y., Li, C., Zeng, Z. (2011): SHRIMP U-Pb (zircon), Ar-Ar (muscovite) and Re-Os (molybdenite) isotopic dating of the Taoxikeng tungsten deposit, South China Block. *Ore Geol. Rev.*, **43**, 26-39.

Kahwage, M.A. & Mendes, J.C. (2003): O berilo gemológico da provincia pegmatitica Oriental do Brasil. *Geochim. Bras.*, **17**, 13-25.

Kortemeier, W.T. & Burt, D.M. (1988): Ongonite and topazite dikes in the Flying W ranch area, Tonto basin, Arizona. *Am. Mineral*., **73**, 507-523.

Launay, G., Sizaret, S., Lach, P., Melleton, J., Gloaguen, E., Poujol, M. (2021): Genetic relationship between greisenization and Sn-W mineralizations in vein and greisen deposits: Insights from the Panasqueira deposit (Portugal). *BSGF - Earth Sci. Bull.*, **192**, 2-29.

Li, L., Chen, Y.J., Qin, J.H. (2009): The Xinqi rare metal multimetallic deposit of syenogranite weathering crust, Tengchong. *Yunnan Geol*., **28**, 72-77.

Martin, R.F. & De Vito, C. (2005): The patterns of enrichment in felsic pegmatites ultimately depend on tectonic setting. *Canad. Mineral*., **43**, 2027.

Martucci, A. & Hansen, T. (2019): Exploring the role of OH/F substitution in topaz: relationships between structural features and chemical environments. Institut Laue-Langevin (ILL). DOI: 10.5291/ILL-DATA.EASY-452.

Monteiro, R.R. & Sabioni, A.C.S. (2014): Preparation of Mullite Whiskers from Powder of Topaz Pure and Doped with Rare Earths. *Mater. Sci. Forum*, **798**, 189-194.

Miao, X. (1999): Porous mullite ceramics from natural topaz. *Mater. Lett*., **38**, 167-172.

Müller-Lorch, D., Marks, M.A.W., Markl, G. (2007): Na and K distribution in agpaitic pegmatites. *Lithos*, **95**, 315-330.

Pedrosa-Soares, A.C., Babinski, M., Noce, C., Martins, M., Queiroga, G., Vilela, F. (2011): The Neoproterozoic Macaúbas Group, Araçuaí orogen, SE Brazil. *Geol. Soc. Lond. Mem*., **36**, 523-534.

Precisvalle, N., Martucci, A., Gigli, L., Plaisier, J.R., Hansen, T.C., Nobre, A.G., Bonadiman, C. (2021): F/OH ratio in a rare fluorine-poor blue topaz from Padre Paraíso (Minas Gerais, Brazil) to unravel topaz's ambient of formation. *Sci. Rep*., **11**, 1-14.

Ribbe, P.H. & Gibbs, G.V. (1971): The crystal structure of topaz and its relation to physical properties. *Am. Mineral*., **56**, 24-30.

Ribbe, P.H. & Rosenberg, P.E. (1971): Optical and X-ray determinative methods for fluorine in topaz. *Am. Mineral*., **56**, 1812-1821.

Soufi, M. (2021): Origin and physical-chemical control of topaz crystallization in felsic igneous rocks: Contrasted effect of temperature on its OH-F substitution. *Earth-Sci. Rev*., **213**, 103467.

Wang, Y., Xing, X., Cawood, P.A., Lai, S., Xia, X., Fan, W., Liu, H., Zhang, F. (2013): Petrogenesis of early Paleozoic peraluminous granite in the Sibumasu Block of SW Yunnan and diachronous accretionary orogenesis along the northern margin of Gondwana. *Lithos*, **182**, 67-85.

Wunder, B., Andrut, M., Wirth, R. (1999): High-pressure synthesis and properties of OH-rich topaz. *Eur. J. Mineral*., **11**, 803-813.

Zagorsky, V.Y., Makagon, V.M., Shmakin, B.M. (1999): The systematics of granitic pegmatites. *Canad. Mineral*., **37**, 800-802.

Zhang, Z.M., Shen, K., Liou, J.G., Dong, X., Wang, W., Yu, F., Liu, F. (2011): Fluid-rock interactions during UHP metamorphism: A review of the Dabie-Sulu orogen, east-central China. *J. Asian Earth Sci*., **42**, 316-329.